10

The HLL and HLLC Riemann Solvers

The approximate Riemann solver proposed by Harten Lax and van Leer (HLL) in 1983 requires estimates for the fastest signal velocities emerging from the initial discontinuity at the interface, resulting in a *two–wave model* for the structure of the exact solution. A more accurate method is the HLLC, introduced by Toro and collaborators in 1992. This method assumes a *three–wave model*, resulting in better resolution of intermediate waves.

10.1 Introduction

For the purpose of computing a Godunov flux, Harten, Lax and van Leer [244] presented a novel approach for solving the Riemann problem approximately. The resulting Riemann solvers have become known as HLL Riemann solvers. In this approach an *approximation for the intercell numerical flux is obtained directly*, unlike the Riemann solvers presented previously in Chaps. 4 and 9. The central idea is to assume, for the solution, a wave configuration that consists of *two waves* separating three constant states. Assuming that the wave speeds are given by some algorithm, application of the integral form of the conservation laws gives a closed–form, approximate expression for the flux. The approach produced practical schemes after the contributions of Davis [150] and Einfeldt [181], who independently proposed various ways of computing the wave speeds required to completely determine the intercell flux. The two–wave HLL approach, along with the wave speed estimates proposed by Einfeldt [181] is known as the HLLE solver. The resulting HLL-type Riemann solvers form the bases of very efficient and robust approximate Godunov–type methods.

One difficulty with these schemes, however, is the assumption of a *two–wave* configuration. This is correct only for hyperbolic systems of two equations, such as the one–dimensional shallow water equations. For larger systems, such as the Euler equations or the split two–dimensional shallow water equations for example, the two–wave assumption is incorrect. As a con-

E.F. Toro, *Riemann Solvers and Numerical Methods for Fluid Dynamics*,
DOI 10.1007/b7976-1_10,

sequence the resolution of physical features such as contact surfaces, shear waves and material interfaces, can be very inaccurate. For the limiting case in which these features are stationary relative to the mesh, the resulting numerical smearing is unacceptable. In view of this situation Einfeldt proposed [181] a modification to the HLLE scheme, called HLLM, in which the single intermediate state in the HLL approach is modified by means of a linear distribution. The modification involves some parameters that control the amount of excessive dissipation for intermediate waves. Particular choices of these parameters and of the wave speed estimates reduce the HLLM scheme to a modified version of the Roe solver. See [182] for further details on both HLLE and HLLEM.

A different approach to remedy the problem of intermediate waves in the HLL approach waves was taken by Toro, Spruce and Speares in 1992 [541], [542]. They proposed the HLLC Riemann solver (C standing for Contact), as applied to the time–dependent Euler equations. HLLC is a three–wave model, resulting two–star states for the intermediate region of the Riemann–problem solution fan. A precursor to HLLC was also anticipated in [505]. Early applications of HLLC include the steady supersonic two–dimensional Euler equations [532] and the time–dependent two dimensional shallow water equations [193], [194]. Batten and collaborators [32] analyzed the HLLC scheme and proposed new ways of estimating the wave speeds. See also the work of Batten, Leschziner and Goldberg [33], in which they proposed implicit versions of the HLLC Riemann solver, with application to turbulent flows. In later work by Linde and others [324], [325] modifications to the HLL two–wave approach were also explored, in order to reduce numerical dissipation of contact waves.

In the last decade or so we have seen further developments of the HLLC method as well as ambitious applications. A quick electronic search, by typing for example *HLLC solver*, will give hundreds of useful entries on the subject. Recall that the Euler equations have *three* distinct characteristic fields in one, two and three space dimensions, see Chapter 3, section 3.2. This is why HLLC as proposed in [541], [542], [96] is a *complete* Riemann solver, for the Euler equations; that is the approximate wave structure of HLLC contains all the characteristic fields of the exact problem. However, for systems with eigenstructure containing more than three distinct characteristic fields, the HLLC becomes *incomplete*, tending to behave like HLL for the one–dimensional Euler equations. The incomplete character of a Riemann solver affects the resolution of intermediate waves, particularly when these move slowly relative to the mesh. Therefore, the obvious way of improving the HLLC approach is to admit the correct number of characteristic fields for the system of interest. Works along these lines include [230], [474] and [75]. Other interesting developments and ambitious applications are found in the following works, to name but a few, [24], [553], [54], [54], [74], [360], [580], [318], [397], [351], [334], [572], [6], [53], [285], [199], [255], [237], [382], [361], [86], [425], [602].

In this Chapter we present the HLL and HLLC Riemann solvers as applied to the three–dimensional, time dependent Euler equations. The principles can

easily be extended to solve other hyperbolic systems. Useful background reading is found in Chaps. 3, 4, 6 and 9. The rest of this chapter is organised as follows: Sect. 10.1 recalls the Riemann problem. In Sect. 10.3 we present the original approach of Harten, Lax and van Leer. In Sect. 10.4 we present the HLLC Riemann solver and in Sect. 10.5 we give various algorithms for computing the required wave speeds. A summary of the HLLC schemes is presented in Sect. 10.6. In Sect. 10.7 we analyse the behaviour of the approximate Riemann solvers in the presence of contacts and passive scalars. Numerical results are shown in Sect. 10.8 and in Sect. 10.9 contains some concluding remarks.

10.2 The Riemann Problem

We are concerned with solving numerically the general Initial Boundary Value Problem (IBVP)

$$\left.\begin{array}{ll} \text{PDEs} : \mathbf{U}_t + \mathbf{F}(\mathbf{U})_x = \mathbf{0} \ , \\ \text{ICs} \quad : \mathbf{U}(x,0) = \mathbf{U}^{(0)}(x) \ , \\ \text{BCs} \quad : \mathbf{U}(0,t) = \mathbf{U}_{\text{l}}(t) \ , \ \mathbf{U}(L,t) = \mathbf{U}_{\text{r}}(t) \ , \end{array}\right\} \tag{10.1}$$

in a domain $0 \leq x \leq L$, with appropriate boundary conditions. We use the explicit conservative formula

$$\mathbf{U}_i^{n+1} = \mathbf{U}_i^n - \frac{\Delta t}{\Delta x}[\mathbf{F}_{i+\frac{1}{2}} - \mathbf{F}_{i-\frac{1}{2}}] \ , \tag{10.2}$$

with the numerical flux $\mathbf{F}_{i+\frac{1}{2}}$ yet to be defined.

10.2.1 The Godunov Flux

In Chap. 6 we defined the Godunov intercell numerical flux as

$$\mathbf{F}_{i+\frac{1}{2}} = \mathbf{F}(\mathbf{U}_{i+\frac{1}{2}}(0)) \ , \tag{10.3}$$

in which $\mathbf{U}_{i+\frac{1}{2}}(0)$ is the exact similarity solution $\mathbf{U}_{i+\frac{1}{2}}(x/t)$ of the Riemann problem

$$\left.\begin{array}{l} \mathbf{U}_t + \mathbf{F}(\mathbf{U})_x = \mathbf{0} \ , \\ \mathbf{U}(x,0) = \left\{ \begin{array}{ll} \mathbf{U}_{\text{L}} & \text{if} \ \ x < 0 \ , \\ \mathbf{U}_{\text{R}} & \text{if} \ \ x > 0 \ , \end{array} \right. \end{array}\right\} \tag{10.4}$$

evaluated at $x/t = 0$. Fig. 10.1 shows the structure of the exact solution of the Riemann problem for the x–split, three dimensional Euler equations, for which the vectors of conserved variables and fluxes are

$$\mathbf{U} = \begin{bmatrix} \rho \\ \rho u \\ \rho v \\ \rho w \\ E \end{bmatrix} \ , \quad \mathbf{F} = \begin{bmatrix} \rho u \\ \rho u^2 + p \\ \rho uv \\ \rho uw \\ u(E+p) \end{bmatrix} \ . \tag{10.5}$$

The value $x/t = 0$ for the Godunov flux corresponds to the t–axis. See Chaps. 4 and 6 for details. The piece–wise constant initial data, in terms of primitive variables, is

$$\mathbf{W}_L = \begin{bmatrix} \rho_L \\ u_L \\ v_L \\ w_L \\ p_L \end{bmatrix} \quad , \quad \mathbf{W}_R = \begin{bmatrix} \rho_R \\ u_R \\ v_R \\ w_R \\ p_R \end{bmatrix} \quad . \tag{10.6}$$

In Chap. 9 we provided approximations to the state $\mathbf{U}_{i+\frac{1}{2}}(x/t)$ and obtained

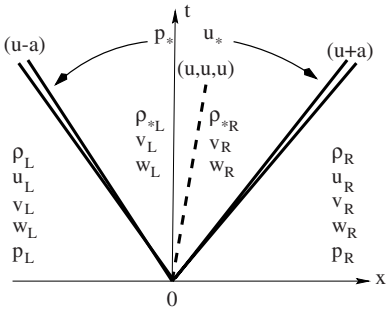

Fig. 10.1. Structure of the exact solution of the Riemann problem for the x–split three dimensional Euler equations. There are five wave families *associated* with the eigenvalues $u - a$, u (of multiplicity 3) and $u + a$.

a corresponding approximate Godunov method by evaluating the physical flux function $\mathbf{F}$ at this approximate state; see (10.3). The purpose of this chapter is to find *direct approximations to the flux function* $\mathbf{F}_{i+\frac{1}{2}}$ following the novel approach proposed by Harten, Lax and van Leer [238].

10.2.2 Integral Relations

Consider Fig. 10.2, in which the whole of the wave structure arising from the exact solution of the Riemann problem is contained in the control volume $[x_L, x_R] \times [0, T]$, that is

$$x_L \leq TS_L \ , \quad x_R \geq TS_R \ , \tag{10.7}$$

where S_L and S_R are the *fastest signal velocities* perturbing the initial data states $\mathbf{U}_L$ and $\mathbf{U}_R$ respectively, and T is a chosen time. The integral form of the conservation laws in (10.4), in the control volume $[x_L, x_R] \times [0, T]$ reads

$$\int_{x_L}^{x_R} \mathbf{U}(x,T)dx = \int_{x_L}^{x_R} \mathbf{U}(x,0)dx + \int_0^T \mathbf{F}(\mathbf{U}(x_L,t))dt - \int_0^T \mathbf{F}(\mathbf{U}(x_R,t))dt \ . \tag{10.8}$$

See Sect. 2.4.1 of Chap. 2 for details on integral forms of conservation laws. Evaluation of the right–hand side of this expression gives

$$\int_{x_L}^{x_R} \mathbf{U}(x,T)dx = x_R\mathbf{U}_R - x_L\mathbf{U}_L + T(\mathbf{F}_L - \mathbf{F}_R) \,, \tag{10.9}$$

where $\mathbf{F}_L = \mathbf{F}(\mathbf{U}_L)$ and $\mathbf{F}_R = \mathbf{F}(\mathbf{U}_R)$. We call the integral relation (10.9) the *consistency condition*. Now we split the integral on the left–hand side of (10.8) into three integrals, namely

$$\int_{x_L}^{x_R} \mathbf{U}(x,T)dx = \int_{x_L}^{TS_L} \mathbf{U}(x,T)dx + \int_{TS_L}^{TS_R} \mathbf{U}(x,T)dx + \int_{TS_R}^{x_R} \mathbf{U}(x,T)dx$$

and evaluate the first and third terms on the right–hand side. We obtain

$$\int_{x_L}^{x_R} \mathbf{U}(x,T)dx = \int_{TS_L}^{TS_R} \mathbf{U}(x,T)dx + (TS_L - x_L)\mathbf{U}_L + (x_R - TS_R)\mathbf{U}_R \,. \tag{10.10}$$

Comparing (10.10) with (10.9) gives

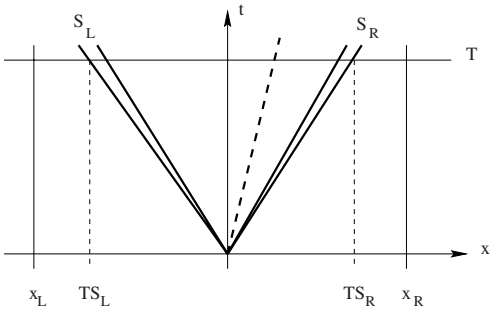

Fig. 10.2. Control volume $[x_L, x_R] \times [0, T]$ on x–t plane. S_L and S_R are the fastest signal velocities arising from the solution of the Riemann problem.

$$\int_{TS_L}^{TS_R} \mathbf{U}(x,T)dx = T(S_R\mathbf{U}_R - S_L\mathbf{U}_L + \mathbf{F}_L - \mathbf{F}_R) \,. \tag{10.11}$$

On division through by the length $T(S_R - S_L)$, which is the width of the wave system of the solution of the Riemann problem between the slowest and fastest signals at time T, we have

$$\frac{1}{T(S_R - S_L)} \int_{TS_L}^{TS_R} \mathbf{U}(x,T)dx = \frac{S_R\mathbf{U}_R - S_L\mathbf{U}_L + F_L - F_R}{S_R - S_L} \,. \tag{10.12}$$

Thus, the integral average of the exact solution of the Riemann problem between the slowest and fastest signals at time T is a known constant, provided

that the signal speeds S_L and S_R are known; such constant is the right–hand side of (10.12) and we denote it by

$$\mathbf{U}^{hll} = \frac{S_R\mathbf{U}_R - S_L\mathbf{U}_L + F_L - F_R}{S_R - S_L} \; . \tag{10.13}$$

We now apply the integral form of the conservation laws to the left portion of Fig. 10.2, that is the control volume $[x_L, 0] \times [0, T]$. We obtain

$$\int_{TS_L}^{0} \mathbf{U}(x,T)dx = -TS_L\mathbf{U}_L + T(\mathbf{F}_L - \mathbf{F}_{0L}) \; , \tag{10.14}$$

where $\mathbf{F}_{0L}$ is the flux $\mathbf{F}(\mathbf{U})$ along the t–axis. Solving for $\mathbf{F}_{0L}$ we find

$$\mathbf{F}_{0L} = \mathbf{F}_L - S_L\mathbf{U}_L - \frac{1}{T}\int_{TS_L}^{0} \mathbf{U}(x,T)dx \; . \tag{10.15}$$

Evaluation of the integral form of the conservation laws on the control volume $[0, x_R] \times [0, T]$ yields

$$\mathbf{F}_{0R} = \mathbf{F}_R - S_R\mathbf{U}_R + \frac{1}{T}\int_{0}^{TS_R} \mathbf{U}(x,T)dx \; . \tag{10.16}$$

The reader can easily verify that the equality

$$\mathbf{F}_{0L} = \mathbf{F}_{0R}$$

results in the *consistency condition* (10.9). All relations so far are exact, as we are assuming the exact solution of the Riemann problem.

10.3 The HLL Approximate Riemann Solver

Harten, Lax and van Leer [244] put forward the following approximate Riemann solver

$$\tilde{\mathbf{U}}(x,t) = \begin{cases} \mathbf{U}_L & \text{if} \quad \frac{x}{t} \le S_L \; , \\ \mathbf{U}^{hll} & \text{if} \quad S_L \le \frac{x}{t} \le S_R \; , \\ \mathbf{U}_R & \text{if} \quad \frac{x}{t} \ge S_R \; , \end{cases} \tag{10.17}$$

where $\mathbf{U}^{hll}$ is the constant state vector given by (10.13) and the speeds S_L and S_R are assumed to be known. Fig. 10.3 shows the structure of this approximate solution of the Riemann problem, called the HLL Riemann solver. Note that this approximation consists of just three constant states separated by two waves. The *Star Region* consists of a *single* constant state; all intermediate states separated by intermediate waves are *lumped* into the single state $\mathbf{U}^{hll}$. The corresponding flux $\mathbf{F}^{hll}$ along the t–axis is found from the relations (10.15) or (10.16), with the exact integrand replaced by the approximate solution (10.17). Note that we *do not take* $\mathbf{F}^{hll} = \mathbf{F}(\mathbf{U}^{hll})$. The non–trivial case of

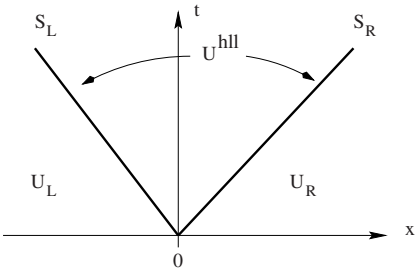

Fig. 10.3. Approximate HLL Riemann solver. Solution in the *Star Region* consists of a single state $\mathbf{U}^{hll}$ separated from data states by two waves of speeds S_L and S_R.

interest is the subsonic case $S_L \leq 0 \leq S_R$. Substitution of the integrand in (10.15) or (10.16) by $\mathbf{U}^{hll}$ in (10.13) gives

$$\mathbf{F}^{hll} = \mathbf{F}_L + S_L(\mathbf{U}^{hll} - \mathbf{U}_L) \,, \tag{10.18}$$

or

$$\mathbf{F}^{hll} = \mathbf{F}_R + S_R(\mathbf{U}^{hll} - \mathbf{U}_R) \,. \tag{10.19}$$

Note that relations (10.18) and (10.19) are also obtained from applying Rankine–Hugoniot conditions across the left and right waves respectively; see Sect. 2.4.2 of Chap. 2 and Sect. 3.1.3 of Chap. 3 for details on the Rankine–Hugoniot conditions. Use of (10.13) in (10.18) or (10.19) gives the HLL flux

$$\mathbf{F}^{hll} = \frac{S_R\mathbf{F}_L - S_L\mathbf{F}_R + S_LS_R(\mathbf{U}_R - \mathbf{U}_L)}{S_R - S_L} \,. \tag{10.20}$$

The corresponding HLL intercell flux for the approximate Godunov method is then given by

$$\mathbf{F}^{hll}_{i+\frac{1}{2}} = \begin{cases} \mathbf{F}_L & \text{if} \quad 0 \leq S_L \,, \\ \dfrac{S_R\mathbf{F}_L - S_L\mathbf{F}_R + S_LS_R(\mathbf{U}_R - \mathbf{U}_L)}{S_R - S_L} \,, & \text{if} \;\; S_L \leq 0 \leq S_R \,, \\ \mathbf{F}_R & \text{if} \quad 0 \geq S_R \,. \end{cases} \tag{10.21}$$

Given an algorithm to compute the speeds S_L and S_R we have an approximate intercell flux (10.21) to be used in the conservative formula (10.2) to produce an approximate Godunov method. Procedures to estimate the wave speeds S_L and S_R are given in Sect. 10.5. Harten, Lax and van Leer [244] showed that the Godunov scheme (10.2), (10.21), if convergent, converges to the weak solution of the conservation laws. In fact they proved that the converged solution is also the physical, entropy satisfying, solution of the conservation laws. Their results actually apply to a larger class of approximate Riemann solvers. One of the requirements is *consistency with the integral form of the conservation laws*.

That is, an approximate solution $\tilde{\mathbf{U}}(x,t)$ is consistent with the integral form of the conservation laws if, when substituted for the exact solution $\mathbf{U}(x,t)$ in the consistency condition (10.9), the right–hand side remains unaltered.

A shortcoming of the HLL scheme is exposed by contact discontinuities, shear waves and material interfaces, or any type of *intermediate waves*. For the Euler equations these waves are associated with the multiple eigenvalue $\lambda_2 = \lambda_3 = \lambda_4 = u$. See Fig. 10.1. Note that in the integral (10.12), all that matters is the average across the wave structure, without regard for the spatial variations of the solution of the Riemann problem in the *Star Region*. As pointed out by Harten, Lax and van Leer themselves [244], this defect of the HLL scheme may be corrected by restoring the missing waves. Accordingly, Toro, Spruce and Speares [541], [542] proposed the so called *HLLC scheme*, where C stands for *Contact*. In this scheme the missing middle waves are put back into the structure of the approximate Riemann solver.

10.4 The HLLC Approximate Riemann Solver

The HLLC scheme is a modification of the HLL scheme described in the previous section, whereby the missing contact and shear waves in the Euler equations are restored. The scheme was first presented in terms of the time–dependent, two dimensional Euler equations [541], [542]. Early applications include the steady supersonic two–dimensional Euler equations [532] and the time–dependent two dimensional shallow water equations [193], [194].

10.4.1 Useful Relations

Consider Fig. 10.2, in which the complete structure of the solution of the Riemann problem is contained in a sufficiently large control volume $[x_L, x_R] \times [0,T]$. Now, in addition to the slowest and fastest signal speeds S_L and S_R we include a middle wave of speed S_*; for the Euler equations this corresponds to the multiple eigenvalue $\lambda_2 = \lambda_3 = \lambda_4 = u$. See Fig. 10.4. Evaluation of the integral form of the conservation laws in the control volume reproduces the result of equation (10.12), even if variations of the integrand across the wave of speed S_* are allowed. Note that the consistency condition (10.9) effectively becomes the condition (10.12). By splitting the left–hand side of integral (10.12) into two terms we obtain

$$\left.\begin{aligned} \frac{1}{T(S_R - S_L)} \int_{TS_L}^{TS_R} \mathbf{U}(x,T)dx = \frac{1}{T(S_R - S_L)} \int_{TS_L}^{TS_*} \mathbf{U}(x,T)dx \\ + \frac{1}{T(S_R - S_L)} \int_{TS_*}^{TS_R} \mathbf{U}(x,T)dx \,. \end{aligned}\right\} \tag{10.22}$$

We define the integral averages

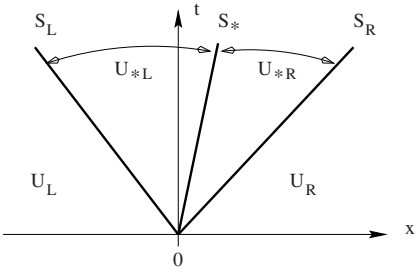

Fig. 10.4. HLLC approximate Riemann solver. Solution in the *Star Region* consists of two constant states separated from each other by a middle wave of speed S_*.

$$\left.\begin{aligned} \mathbf{U}_{*L} &= \frac{1}{T(S_* - S_L)} \int_{TS_L}^{TS_*} \mathbf{U}(x,T)dx \ , \\ \mathbf{U}_{*R} &= \frac{1}{T(S_R - S_*)} \int_{TS_*}^{TS_R} \mathbf{U}(x,T)dx \ . \end{aligned}\right\} \tag{10.23}$$

By substitution of (10.23) into (10.22) and use of (10.12), the consistency condition (10.9) becomes

$$\left(\frac{S* - S_L}{S_R - S_L}\right)\mathbf{U}_{*L} + \left(\frac{S_R - S_*}{S_R - S_L}\right)\mathbf{U}_{*R} = \mathbf{U}^{hll} \ , \tag{10.24}$$

where $\mathbf{U}^{hll}$ is given by (10.12)–(10.13). The HLLC approximate Riemann solver is given as follows

$$\tilde{\mathbf{U}}(x,t) = \begin{cases} \mathbf{U}_L & \text{, if } \ \frac{x}{t} \le S_L \ , \\ \mathbf{U}_{*L} & \text{, if } S_L \le \frac{x}{t} \le S_* \ , \\ \mathbf{U}_{*R} & \text{, if } S_* \le \frac{x}{t} \le S_R \ , \\ \mathbf{U}_R & \text{, if } \ \frac{x}{t} \ge S_R \ . \end{cases} \tag{10.25}$$

We seek a corresponding HLLC numerical flux defined as

$$\mathbf{F}_{i+\frac{1}{2}}^{hllc} = \begin{cases} \mathbf{F}_L & \text{, if } \ 0 \le S_L \ , \\ \mathbf{F}_{*L} & \text{, if } S_L \le 0 \le S_* \ , \\ \mathbf{F}_{*R} & \text{, if } S_* \le 0 \le S_R \ , \\ \mathbf{F}_R & \text{, if } \ 0 \ge S_R \ , \end{cases} \tag{10.26}$$

with the intermediate fluxes $\mathbf{F}_{*L}$ and $\mathbf{F}_{*R}$ still to be determined. Fig. 10.4 shows the structure of the HLLC approximate Riemann solver.

By integrating over appropriate control volumes, or more directly, by applying Rankine–Hugoniot Conditions across each of the waves of speeds S_L, S_*, S_R, we obtain

$$\mathbf{F}_{*L} = \mathbf{F}_L + S_L(\mathbf{U}_{*L} - \mathbf{U}_L) \ , \tag{10.27}$$

$$\mathbf{F}_{*R} = \mathbf{F}_{*L} + S_*(\mathbf{U}_{*R} - \mathbf{U}_{*L}) \ , \tag{10.28}$$

$$\mathbf{F}_{*R} = \mathbf{F}_R + S_R(\mathbf{U}_{*R} - \mathbf{U}_R) \ . \tag{10.29}$$

Compare relations (10.27) and (10.29) for the HLLC scheme with (10.18) and (10.19) for the HLL scheme. Substitution of $\mathbf{F}_{*L}$ from (10.27) and $\mathbf{F}_{*R}$ from (10.29) into (10.28) gives identically the consistency condition (10.24). Hence conditions (10.27)–(10.29) are sufficient for ensuring consistency; these are three equations for the four unknowns vectors $\mathbf{U}_{*L}$, $\mathbf{F}_{*L}$, $\mathbf{U}_{*R}$, $\mathbf{F}_{*R}$.

10.4.2 The HLLC Flux for the Euler Equations

We seek the solution for the two unknown intermediate fluxes $\mathbf{F}_{*L}$ and $\mathbf{F}_{*R}$. From (10.27)–(10.29) we see that it is sufficient to find solutions for the two intermediate state vectors $\mathbf{U}_{*L}$ and $\mathbf{U}_{*R}$. There are more unknowns than equations and some extra conditions need to be imposed, in order to solve the algebraic problem. Obvious conditions to impose are those satisfied by the exact solution; for pressure and normal component of velocity we have

$$\left.\begin{array}{l} p_{*L} = p_{*R} = p_* \ , \\ u_{*L} = u_{*R} = u_* \ , \end{array}\right\} \tag{10.30}$$

and for tangential velocity components we have

$$\left.\begin{array}{l} v_{*L} = v_L \ \ , \ v_{*R} = v_R \ , \\ w_{*L} = w_L \ \ , \ w_{*R} = w_R \ . \end{array}\right\} \tag{10.31}$$

See Chap. 4. In addition, it is entirely justified, and convenient, to set

$$S_* = u_* \tag{10.32}$$

and thus if an estimate for S_* is known, the normal velocity component u_* in the *Star Region* is known. Now equations (10.27) and (10.29) can be re–arranged as

$$S_L\mathbf{U}_{*L} - \mathbf{F}_{*L} = S_L\mathbf{U}_L - \mathbf{F}_L \ , \tag{10.33}$$

and

$$S_R\mathbf{U}_{*R} - \mathbf{F}_{*R} = S_R\mathbf{U}_R - \mathbf{F}_R \ , \tag{10.34}$$

where the right–hand sides of (10.33) and (10.34) are known constant vectors. We also note the useful relation between $\mathbf{U}$ and $\mathbf{F}$, namely

$$\mathbf{F}(\mathbf{U}) = u\mathbf{U} + p\mathbf{D} \ , \quad \mathbf{D} = [0, 1, 0, 0, u]^T \ . \tag{10.35}$$

Assuming that the wave speeds S_L and S_R are known and performing algebraic manipulations of the first and second components of equations (10.33)–(10.34) one obtains the following solutions for pressure in the two *Star Regions*

$$p_{*L} = p_L + \rho_L(S_L - u_L)(S_* - u_L) \ , \quad p_{*R} = p_R + \rho_R(S_R - u_R)(S_* - u_R) \ . \tag{10.36}$$

From (10.30) $p_{*L} = p_{*R}$, which from (10.36) allows us to obtain an expression for the speed S_* purely in terms of the assumed speeds S_L and S_R, namely

$$S_* = \frac{p_R - p_L + \rho_L u_L(S_L - u_L) - \rho_R u_R(S_R - u_R)}{\rho_L(S_L - u_L) - \rho_R(S_R - u_R)} \ . \tag{10.37}$$

Thus, we only need to provide estimates for S_L and S_R, just as for the simpler HLL solver.

Algebraic manipulation of (10.33) and (10.34) and using the corresponding values p_{*L} and p_{*R} from (10.36) gives the intermediate fluxes $\mathbf{F}_{*L}$ and $\mathbf{F}_{*R}$ as

$$\mathbf{F}_{*K} = \mathbf{F}_K + S_K(\mathbf{U}_{*K} - \mathbf{U}_K) \ , \tag{10.38}$$

for K=L and K=R, with the intermediate states given as

$$\mathbf{U}_{*K} = \rho_K \left(\frac{S_K - u_K}{S_K - S_*} \right) \begin{bmatrix} 1 \\ S_* \\ v_K \\ w_K \\ \dfrac{E_K}{\rho_K} + (S_* - u_K) \left[S_* + \dfrac{p_K}{\rho_K(S_K - u_K)} \right] \end{bmatrix} . \tag{10.39}$$

The final choice of the HLLC flux is made according to (10.26).

A variation in the formulation of the HLLC solver (10.38)–(10.39) is the following. From equations (10.33) and (10.34) we may write the following solutions for the state vectors $\mathbf{U}_{*L}$ and $\mathbf{U}_{*R}$

$$\mathbf{U}_{*K} = \frac{S_K \mathbf{U}_K - \mathbf{F}_K + p_{*K}\mathbf{D}_*}{S_L - S_*} \quad , \quad \mathbf{D}_* = [0, 1, 0, 0, S_*] \ , \tag{10.40}$$

with p_{*L} and p_{*R} as given by (10.36). Substitution of p_{*K} from (10.36) into (10.40) followed by use of (10.27) and (10.29) gives direct expressions for the intermediate fluxes as

$$\mathbf{F}_{*K} = \frac{S_*(S_K \mathbf{U}_K - \mathbf{F}_K) + S_K(p_K + \rho_L(S_K - u_K)(S_* - u_K))D_*}{S_K - S_*} \ , \tag{10.41}$$

with the final choice of the HLLC flux made again according to (10.26).

We remark here that the HLLC formulation (10.38)–(10.39) enforces the condition $p_{*L} = p_{*R}$, which is satisfied by the exact solution. In the alternative HLLC formulation (10.41) we relax such condition, being more consistent with the pressure approximations (10.36).

A different HLLC flux is obtained by assuming a single mean pressure value in the *Star Region*, and given by the arithmetic average of the pressures in (10.36), namely

$$P_{LR} = \frac{1}{2}[p_L + p_R + \rho_L(S_L - u_L)(S_* - u_L) + \rho_R(S_R - u_R)(S_* - u_R)] \ . \quad (10.42)$$

Then the intermediate state vectors are given by

$$\mathbf{U}_{*K} = \frac{S_K \mathbf{U}_K - \mathbf{F}_K + P_{LR}\mathbf{D}_*}{S_K - S_*} \ . \quad (10.43)$$

Substitution of these into (10.27) and (10.29) gives the fluxes $\mathbf{F}_{*L}$ and $\mathbf{F}_{*R}$ as

$$\mathbf{F}_{*K} = \frac{S_*(S_K \mathbf{U}_K - \mathbf{F}_K) + S_K P_{LR}\mathbf{D}_*}{S_K - S_*} \ . \quad (10.44)$$

Again the final choice of HLLC flux is made according to (10.26).

Remark: general equation of state. All manipulations so far, assuming that wave speed estimates for S_L and S_R are available, are valid for any equation of state. The equation of state only enters in prescribing estimates for S_L and S_R.

10.4.3 Multidimensional and Multicomponent Flow

Here we consider extensions of the HLLC solver to two areas of application, namely multidimensional flow and multicomponent flow.

The presentation of the HLLC scheme has been made for the x–split three–dimensional Euler equations, for which the corresponding eigenvalues are denoted here as $\lambda_1 = u - a$, $\lambda_2 = u$ (multiplicity 3), $\lambda_3 = u + a$, where u is the *normal* velocity component and a is the speed of sound. In a general multidimensional situation, see Chapt. 16, one usually requires the flux in the direction *normal* to a volume (or element) interface, which is not necessarily aligned with any of the Cartesian directions. In this case the form of the governing equations remains identical to the x–split system (10.4), (10.5). There will be a normal and two tangential components of velocity as before, and all the results obtained so far will be applicable.

In the study of multicomponent flow, one considers the advection of *chemical species* by the flow, the carrier fluid. For example, let us consider m species of concentrations q_l, for $l = 1, \ldots, m$, advected with the normal fluid speed u. This means that for each species we can write the following advection equation

$$\partial_t q_l + u\partial_x q_l = 0 \ ,$$

for $l = 1, \ldots, m$. Note that these equations are written in non–conservative form. However, by combining these with the continuity equation we obtain a conservative form of these equations, namely

$$(\rho q_l)_t + (\rho u q_l)_x = 0 \ , \text{ for } l = 1, \ldots, m \ .$$

The eigenvalues of the enlarged system are as before, with the exception of $\lambda_2 = u$, which now, in three space dimensions, has multiplicity $m + 3$. These conservation equations can then be added as new components to the conservation equations in (10.1) or (10.4), with the enlarged vectors of conserved variables and fluxes given as

$$\mathbf{U} = \begin{bmatrix} \rho \\ \rho u \\ \rho v \\ \rho w \\ E \\ \rho q_1 \\ \cdots \\ \rho q_l \\ \cdots \\ \rho q_m \end{bmatrix}, \quad \mathbf{F} = \begin{bmatrix} \rho u \\ \rho u^2 + p \\ \rho uv \\ \rho uw \\ u(E+p) \\ \rho u q_1 \\ \cdots \\ \rho u q_l \\ \cdots \\ \rho u q_m \end{bmatrix}. \tag{10.45}$$

The HLLC flux accommodates these new equations in a very natural way, and nothing special needs to be done. If the HLLC flux (10.38) is used, with $\mathbf{F}$ as in (10.45), then the intermediate state vectors are given by

$$\mathbf{U}_{*K} = \rho_K \left(\frac{S_K - u_K}{S_K - S_*} \right) \begin{bmatrix} 1 \\ S_* \\ v_K \\ w_K \\ \dfrac{E_K}{\rho_K} + (S_* - u_K) \left[S_* + \dfrac{p_K}{\rho_K (S_K - u_K)} \right] \\ (q_1)_K \\ \cdots \\ (q_l)_K \\ \cdots \\ (q_m)_K \end{bmatrix}. \tag{10.46}$$

for $K = L$ and $K = R$. In this manner the HLLC flux will resolve the additional intermediate fields as the exact Riemann solver.

Note that the tangential velocity components v and w are special cases of passive scalars; compare (10.46) with (10.39) for $q = v$ and $q = w$.

10.5 Wave–Speed Estimates

In order to determine completely the numerical fluxes in both the HLL and HLLC Riemann solvers we need to provide an algorithm for computing the wave speeds S_L and S_R. For the HLLC scheme one requires in addition an estimate for the speed of the middle wave S_*, but as seen in (10.37), this can in fact be computed once S_L and S_R are known. Thus the pending task is to

determine estimates for S_L and S_R. One approach is to estimate the speeds directly; another approach relies on pressure estimates in the *Star Region*, which are then utilised to obtain S_L and S_R using exact wave relations.

10.5.1 Direct Wave Speed Estimates

The most well known approach for estimating bounds for the minimum and maximum signal velocities present in the solution of the Riemann problem is to provide, directly, wave speeds S_L and S_R. Davis [150] suggested the simple estimates

$$S_L = u_L - a_L \ , \quad S_R = u_R + a_R \tag{10.47}$$

and

$$S_L = \min\{u_L - a_L, u_R - a_R\} \ , \quad S_R = \max\{u_L + a_L, u_R + a_R\} \ . \tag{10.48}$$

These estimates make use of data values only, are exceedingly simple but are not recommended for practical computations. Both Davis [150] and Einfeldt [181], proposed to use the Roe [407] average eigenvalues for the left and right non–linear waves, that is

$$S_L = \tilde{u} - \tilde{a} \ , \quad S_R = \tilde{u} + \tilde{a} \ , \tag{10.49}$$

where $\tilde{u}$ and $\tilde{a}$ are the Roe–average particle and sound speeds respectively, given as follows

$$\tilde{u} = \frac{\sqrt{\rho_L}u_L + \sqrt{\rho_R}u_R}{\sqrt{\rho_L} + \sqrt{\rho_R}} \ , \quad \tilde{a} = \left[(\gamma - 1)(\tilde{H} - \frac{1}{2}\tilde{u}^2)\right]^{1/2} \ , \tag{10.50}$$

with the enthalpy $H = (E + p)/\rho$ approximated as

$$\tilde{H} = \frac{\sqrt{\rho_L}H_L + \sqrt{\rho_R}H_R}{\sqrt{\rho_L} + \sqrt{\rho_R}} \ . \tag{10.51}$$

Complete details of the Roe Riemann solver are given in Chap. 11.

Motivated by the Roe eigenvalues Einfeldt [181] proposed the estimates

$$S_L = \bar{u} - \bar{d} \ , \quad S_R = \bar{u} + \bar{d} \ , \tag{10.52}$$

for his HLLE solver, where

$$\bar{d}^2 = \frac{\sqrt{\rho_L}a_L^2 + \sqrt{\rho_R}a_R^2}{\sqrt{\rho_L} + \sqrt{\rho_R}} + \eta_2(u_R - u_L)^2 \tag{10.53}$$

and

$$\eta_2 = \frac{1}{2}\frac{\sqrt{\rho_L}\sqrt{\rho_R}}{(\sqrt{\rho_L} + \sqrt{\rho_R})^2} \ . \tag{10.54}$$

These wave speed estimates are reported to lead to effective and robust Godunov–type schemes. More details on the HLLE solver and its modification HLLEM, are found in [182]. In this paper the authors also analyze the effect of the choice of wave speed estimates on the Riemann solver and introduce the concept of *positively conservative* Riemann solvers, for the Euler equations. These are solvers for which, for physically admissible data, density and internal energy remain positive during the calculations. See Batten et al. [32] for further discussion on direct wave speed estimates.

Davis made some observations regarding the relationship between the chosen wave speeds and some well–known numerical methods. Suppose that for a given Riemann problem we can identify a positive speed S^+. Then by choosing $S_L = -S^+$ and $S_R = S^+$ in the HLL flux (10.20) one obtains a Rusanov flux [418]

$$\mathbf{F}_{i+1/2} = \frac{1}{2}(\mathbf{F}_L + \mathbf{F}_R) - \frac{1}{2}S^+(\mathbf{U}_R - \mathbf{U}_L) \; . \tag{10.55}$$

As to the choice of the speed S^+, Davis [150] considered

$$S^+ = \max\{\mid u_L - a_L \mid, \mid u_R - a_R \mid, \mid u_L + a_L \mid \; , \mid u_R + a_R \mid\} \; .$$

Actually, the above speed is bounded by

$$S^+ = \max\{\mid u_L \mid + a_L, \mid u_R \mid + a_R\} \; . \tag{10.56}$$

This choice is likely to produce a more robust scheme and is also simpler than Davis's choice.

Another possible choice is $S^+ = S^n_{max}$, the maximum wave speed present at the appropriate time found by imposing the Courant stability condition; see Sect. 6.3.2 of Chap. 6. This speed is related to the time step Δt and the grid spacing Δx via

$$S^n_{max} = \frac{C_{cfl}\Delta x}{\Delta t} \; , \tag{10.57}$$

where C_{cfl} is the Courant number coefficient, usually chosen (empirically) to be $C_{cfl} \approx 0.9$, for a scheme of linear stability limit of unity. For $C_{cfl} = 1$ one has $S^+ = \frac{\Delta x}{\Delta t}$, which results in the Lax–Friedrichs numerical flux

$$F_{i+1/2} = \frac{1}{2}(F_L + F_R) - \frac{1}{2}\frac{\Delta x}{\Delta t}(U_R - U_L) \; . \tag{10.58}$$

See Sect. 5.3.4 of Chap. 5 and Sect. 7.3.1 of Chap. 7.

In the next section we propose a different way of finding wave–speed estimates.

10.5.2 Pressure–Based Wave Speed Estimates

A different approach for finding wave speed estimates was proposed by Toro et. al. [542], whereby one first finds an estimate for the pressure p_* in

the *Star Region*. Then, estimates for S_L and S_R are derived. This is a simple task and several reliable choices are available. Suppose we have an estimate p_* for the pressure in the *Star Region*. Then we choose the following wave speeds

$$S_L = u_L - a_L q_L \ , \quad S_R = u_R + a_R q_R \ , \tag{10.59}$$

where

$$q_K = \begin{cases} 1 & \text{if} \quad p_* \le p_K \\ \left[1 + \dfrac{\gamma+1}{2\gamma}(p_*/p_K - 1)\right]^{1/2} & \text{if} \quad p_* > p_K \ . \end{cases} \tag{10.60}$$

This choice of wave speeds discriminates between shock and rarefaction waves. If the K wave ($K = L$ or $K = R$) is a rarefaction then the speed S_K corresponds to the characteristic speed of the head of the rarefaction, which carries the fastest signal. If the wave is a shock wave then the speed corresponds to an approximation of the true shock speed; the wave relations used are exact but the pressure ratio across the shock is approximated, because p_* is an approximation to the pressure behind the shock wave. We propose to use the state approximations of Chap. 9 to find p_*.

The PVRS approximate Riemann solver [502] presented in Sect. 9.3 of Chap. 9 gives

$$p_{pvrs} = \frac{1}{2}(p_L + p_R) - \frac{1}{2}(u_R - u_L)\bar{\rho}\bar{a} \ , \tag{10.61}$$

where

$$\bar{\rho} = \frac{1}{2}(\rho_L + \rho_R) \ , \quad \bar{a} = \frac{1}{2}(a_L + a_R) \ . \tag{10.62}$$

This approximation for pressure can be used directly into (10.59)–(10.60) to obtain wave speed estimates for the HLL and HLLC schemes. See also Eq. (9.28) of Chapt. 9 for alternative estimates for p_*.

Another choice is furnished by the Two–Rarefaction Riemann solver TRRS of Sect. 9.4.1 of Chap. 9, namely

$$p_{tr} = \left[\frac{a_L + a_R - \frac{\gamma-1}{2}(u_R - u_L)}{a_L/p_L^z + a_R/p_R^z}\right]^{1/z} \ , \tag{10.63}$$

where

$$P_{LR} = \left(\frac{p_L}{p_R}\right)^z \ ; \quad z = \frac{\gamma-1}{2\gamma} \ . \tag{10.64}$$

The Two–Shock Riemann solver TSRS of Sect. 9.4.2 of Chap. 9 gives

$$p_{ts} = \frac{g_L(p_0)p_L + g_R(p_0)p_R - \Delta u}{g_L(p_0) + g_R(p_0)} \ , \tag{10.65}$$

where

$$g_K(p) = \left[\frac{A_K}{p + B_K}\right]^{1/2} , \quad p_0 = max(0, p_{pvrs}) , \tag{10.66}$$

for $K = L$ and $K = R$.

In computational practice we could use the hybrid scheme of Sect. 9.5.2 of Chap. 9 to determine p_* See Chap. 9 for full details. The HLL approximate Riemann solver with the hybrid pressure–based wave speed estimates has been implemented in the NAG routine D03PXF [319] for Godunov–type methods to solve the time–dependent, one dimensional Euler equations for ideal gases. For ideal gases we find that the simplified PVRS scheme, with $p_* = max(0, p_{pvrs})$ is very simple and also is found to be sufficiently robust.

10.6 Summary of HLLC Fluxes

Here we summarize the HLLC scheme, based on a particular choice of wave speeds. To compute the HLLC flux one performs the following steps:

- *Step I: pressure estimate.* Compute estimate for the pressure p_* in the *Star Region* as

$$\left.\begin{aligned} p_* = max(0, p_{pvrs}) , \quad p_{pvrs} = \tfrac{1}{2}(p_L + p_R) - \tfrac{1}{2}(u_R - u_L)\bar{\rho}\bar{a} , \\ \bar{\rho} = \tfrac{1}{2}(\rho_L + \rho_R) , \quad \bar{a} = \tfrac{1}{2}(a_L + a_R) . \end{aligned}\right\} \tag{10.67}$$

  There are other possible choices for estimating the pressure p_*. See (10.63) and (10.65).
- *Step II: wave speed estimates.* Compute the wave speed estimates for S_L and S_R as

$$S_L = u_L - a_L q_L , \quad S_R = u_R + a_R q_R , \tag{10.68}$$

  with

$$q_K = \begin{cases} 1 & \text{if } p_* \le p_K \\ \left[1 + \dfrac{\gamma + 1}{2\gamma}(p_*/p_K - 1)\right]^{1/2} & \text{if } p_* > p_K . \end{cases} \tag{10.69}$$

  Then compute the intermediate speed S_* in terms of S_L and S_R as

$$S_* = \frac{p_R - p_L + \rho_L u_L(S_L - u_L) - \rho_R u_R(S_R - u_R)}{\rho_L(S_L - u_L) - \rho_R(S_R - u_R)} . \tag{10.70}$$

  Other choices of S_L and S_R are possible. See for example (10.49) and (10.52)

- *Step III: HLLC flux.* Compute the HLLC flux, according to

$$\mathbf{F}_{i+\frac{1}{2}}^{hllc} = \begin{cases} \mathbf{F}_L & \text{if} \quad 0 \le S_L \ , \\ \mathbf{F}_{*L} & \text{if} \quad S_L \le 0 \le S_* \ , \\ \mathbf{F}_{*R} & \text{if} \quad S_* \le 0 \le S_R \ , \\ \mathbf{F}_R & \text{if} \quad 0 \ge S_R \ , \end{cases} \tag{10.71}$$

with

$$\mathbf{F}_{*K} = \mathbf{F}_K + S_K(\mathbf{U}_{*K} - \mathbf{U}_K) \tag{10.72}$$

and

$$\mathbf{U}_{*K} = \rho_K \left(\frac{S_K - u_K}{S_K - S_*} \right) \begin{bmatrix} 1 \\ S_* \\ v_K \\ w_K \\ \dfrac{E_K}{\rho_K} + (S_* - u_K) \left[S_* + \dfrac{p_K}{\rho_K (S_K - u_K)} \right] \end{bmatrix} . \tag{10.73}$$

There are two variants of the HLLC flux in the third step, as seen below.

- *Step III: HLLC flux, Variant 1.* Compute the numerical fluxes as

$$\left. \begin{aligned} \mathbf{F}_{*K} &= \frac{S_*(S_K \mathbf{U}_K - \mathbf{F}_K) + S_K(p_K + \rho_L(S_K - u_K)(S_* - u_K))\mathbf{D}_*}{S_K - S_*} \ , \\ \mathbf{D}_* &= [0, 1, 0, 0, S_*]^T \ , \end{aligned} \right\} \tag{10.74}$$

and the final HLLC flux chosen according to (10.71).

- *Step III: HLLC flux, Variant 2.* Compute the numerical fluxes as

$$\mathbf{F}_{*K} = \frac{S_*(S_K \mathbf{U}_K - \mathbf{F}_K) + S_K P_{LR} \mathbf{D}_*}{S_K - S_*} \ , \tag{10.75}$$

with $\mathbf{D}_*$ as in (10.74) and

$$P_{LR} = \frac{1}{2}[p_L + p_R + \rho_L(S_L - u_L)(S_* - u_L) + \rho_R(S_R - u_R)(S_* - u_R)] \ . \tag{10.76}$$

The final HLLC flux is chosen according to (10.71).

10.7 Contact Waves and Passive Scalars

Here we study the special case of a passive scalar $q(x,t)$ transported with the fluid speed $u(x,t)$. The time–dependent, one dimensional Euler equations are augmented by the extra conservation law

$$(\rho q)_t + (\rho q u)_x = 0 \ . \tag{10.77}$$

Consider the special IVP in which $p = constant$, $\rho = constant$, $u = constant$ and

$$q(x,0) = q_0(x) = \begin{cases} q_L & \text{if } \ x \leq 0 \ , \\ q_R & \text{if } \ x > 0 \ . \end{cases} \tag{10.78}$$

Clearly, the non–trivial part of the exact solution is

$$q(x,t) = q_0(x - ut) \ . \tag{10.79}$$

Application of the HLL Riemann solver to this problem gives the following expression for the numerical flux

$$f^{hll}_{i+\frac{1}{2}} = \frac{1}{2}\left(1 + \frac{1}{M}\right) f_i + \frac{1}{2}\left(1 - \frac{1}{M}\right) f_{i+1} \ , \tag{10.80}$$

where $M = \frac{u}{a}$ is the Mach number and the wave speeds have been taken to be

$$S_L = u - a \ , \quad S_R = u + a \ .$$

Obviously, this flux applies only in the subsonic regime $u - a \leq 0 \leq u + a$. For sonic flow, the flux (10.80) reduces identically to the Godunov flux computed from the exact Riemann solver. For subsonic flow $1/M > 1$ and the resulting scheme is *more diffusive than the Godunov method* when used in conjunction with the exact Riemann solver. For the special case

$$M = \frac{u\Delta t}{\Delta x}$$

the HLL scheme reproduces the Lax–Friedrichs method, which is exceedingly diffusive, see Chaps. 5 and 6. The limiting case of a stationary passive scalar is the worst. Note that the analysis includes the important cases $q = v$ and $q = w$, the tangential velocity components in three–dimensional flow.

The analysis for an isolated contact can be carried out in a similar manner; by using an appropriate choice of the wave speeds the resulting HLL flux is identical to (10.80), and thus the same observations as for a passive scalar apply. The HLLC solver, on the other hand, behaves as the exact Riemann solver; for the limiting case in which the wave is stationary, the HLLC numerical scheme gives infinite resolution; the reader can verify this algebraically. In the next section on numerical results we compare the HLL and HLLC schemes for this type of problems; see Fig. 10.9. The relevance of these observations is that the HLL scheme, unlike the HLLC scheme, will add excessive numerical dissipation to the resolution of special but important flow features such as material interfaces, shear waves and vortices.

10.8 Numerical Results

Here we assess the performance of Godunov's first–order method used in conjunction with the HLL and HLLC approximate Riemann solvers presented in this chapter. The HLLC results shown correspond to the version (10.38)–(10.39). For both HLL and HLLC, the wave speed estimates for S_L and S_R are based on a pressure estimate obtained from the adaptive scheme of section 9.5.2 of Chapter 9. For HLLC we note that, for the tests considered, all three versions of HLLC give identical results when using the simple algorithm (10.67)–(10.70).

We select seven test problems for the one–dimensional, time dependent Euler equations for ideal gases with $\gamma = 1.4$; these have exact solutions. In all chosen tests, data consists of two constant states $\mathbf{W}_{\rm L} = [\rho_{\rm L}, u_{\rm L}, p_{\rm L}]^T$ and $\mathbf{W}_{\rm R} = [\rho_{\rm R}, u_{\rm R}, p_{\rm R}]^T$, separated by a discontinuity at a position $x = x_0$. The states $\mathbf{W}_{\rm L}$ and $\mathbf{W}_{\rm R}$ are given in Table 10.1. The exact and numerical solutions are found in the spatial domain $0 \le x \le 1$. The numerical solution is computed with $M = 100$ cells and the CFL condition is as for all previous computations, see Chap. 6; the chosen Courant number coefficient is $C_{\rm cfl} = 0.9$; boundary conditions are transmissive.

The exact solutions were found by running the code HE-E1RPEXACT of the library *NUMERICA* [518] and the numerical solutions were obtained by running the code HE-E1GODFLUX of *NUMERICA*.

Test	$\rho_{\rm L}$	$u_{\rm L}$	$p_{\rm L}$	$\rho_{\rm R}$	$u_{\rm R}$	$p_{\rm R}$
1	1.0	0.75	1.0	0.125	0.0	0.1
2	1.0	-2.0	0.4	1.0	2.0	0.4
3	1.0	0.0	1000.0	1.0	0.0	0.01
4	5.99924	19.5975	460.894	5.99242	-6.19633	46.0950
5	1.0	-19.59745	1000.0	1.0	-19.59745	0.01
6	1.4	0.0	1.0	1.0	0.0	1.0
7	1.4	0.1	1.0	1.0	0.1	1.0

Table 10.1. Data for seven test problems with exact solution

Test 1 is a *modified* version of Sod's problem [453]; the solution has a right shock wave, a right travelling contact wave and a left *sonic* rarefaction wave; this test is useful for assessing the *entropy satisfaction* property of numerical methods. The solution of Test 2 consists of two symmetric rarefaction waves and a trivial contact wave; the *Star Region* between the non–linear waves is close to vacuum, which makes this problem a suitable test for assessing the performance of numerical methods for low–density flows. Test 3 is designed to assess the robustness and accuracy of numerical methods; its solution consists of a strong shock wave of shock Mach number 198, a contact surface and a left rarefaction wave. Test 4 is also a very severe test, its solution consists of three strong discontinuities travelling to the right. A detailed discussion on the

exact solution of Tests 1 to 4 is found in Sect. 4.3.3 of Chap. 4. Test 5 is also designed to test the robustness of numerical methods but the main reason for devising this test is to assess the ability of the numerical methods to resolve *slowly–moving contact discontinuities*. The exact solution of Test 5 consists of a left rarefaction wave, a right–travelling shock wave and a *stationary* contact discontinuity. Test 6 corresponds to an isolated stationary contact wave and Test 7 corresponds to an isolated contact moving slowly to the right. The purpose of Tests 6 and 7 is to illustrate the likely performance of HLL and HLLC for contacts, shear waves and vortices. For each test problem we select a convenient position x_0 of the initial discontinuity and the output time. These are stated in the legend of each figure displaying computational results.

We compare computed results with the exact solution for three first–order methods, namely the Godunov method used in conjunction with the HLL and HLLC approximate Riemann solvers, and the Rusanov scheme. In all three schemes we compute wave speed estimates by using the adaptive noniterative scheme of Sect. 9.5.2 of Chapt. 9. Figs. 10.5 to 10.9 show results for Godunov's method with the HLLC Riemann solver. Figs. 10.10 to 10.14 show results for the Godunov method with the HLL Riemann solver and Figs. 10.15 to 10.19 show results for Rusanov's method. Fig. 10.20 shows results aimed at comparing the performance of HLL and HLLC for isolated, stationary and slowly moving contact discontinuities.

The numerical results obtained from the Godunov method in conjunction with the HLL and HLLC approximate Riemann solvers are broadly similar to those obtained from Godunov's method in conjunction with the exact Riemann solver. See results of Chapt. 6. Some points to note are the following: the *sonic rarefaction* of Test 1 is better resolved by the HLL and HLLC approximate Riemann solvers than by the exact Riemann solver. The resolution of the stationary contact (non–isolated) of Test 5 by the HLLC Riemann solver is comparable with that of the exact Riemann solver. The HLL Riemann solver however, as anticipated by the analysis of Sect. 10.7, diffuses the contact wave to similar levels seen in the Flux Vector Splitting methods of Steger–Warming and van Leer, see results of Chap. 8. The advantage of HLLC over HLL is the resolution of slowly–moving contact discontinuities; this point is further emphasised by the results of Tests 6 and 7 for an *isolated* contact wave. The HLLC Riemann solver preserves the excellent entropy–satisfaction property of the HLL Riemann solver. The Rusanov scheme is broadly similar to the HLL Riemann solver in that it also diffuses slowly moving contacts. For Test 1 containing a sonic rarefaction however, the Rusanov scheme is clearly inferior to the HLL scheme, compare Fig. 10.15 with Fig. 10.10.

The results of Tests 6 and 7 using both the HLL and the HLLC schemes are shown in Fig. 10.20. As anticipated by the analysis of Sect. 10.7, the HLL scheme will give unacceptably smeared results for stationary and slowly moving contact waves. The HLLC behaves like the exact Riemann solver for this type of problem; it has much less numerical dissipation for slowly moving contacts and it gives infinite resolution for stationary contact waves. The

same observations apply to augmented systems of equations containing species equations, and to shear waves and vortices in multiple space dimensions.

10.9 Closing Remarks

We have first studied HLL and HLLC approximate Riemann solvers for the split three–dimensional Euler equations. Then we have indicated the manner in which these solvers can be extended to three–dimensional flow and to multicomponent flow, noting that HLLC will perform as the exact Riemann solver in these more general situations. This is due to the fact that tangential velocity components and species concentrations are all represented by the intermediate characteristic field $\lambda_2 = u$, where u is understood as the normal velocity component. HLLC, unlike HLL, captures correctly this characteristic field, which is enough to correctly capture contact discontinuities, shear waves and contact discontinuities associated with all the species equations.

The approximate Riemann solvers of this chapter may be applied in conjunction with the Godunov first–order upwind method presented in Chap. 6. Second–order Total Variation Diminishing (TVD) extensions of the schemes are presented in Chap. 13 for scalar problems and in Chap. 14 for non–linear one dimensional systems. In Chap. 15 we present techniques that allow the extension of these schemes to solve problems with source terms. In Chap. 16 we study techniques to extend the methods of this chapter to three–dimensional problems. Implicit versions of the HLL and HLLC Riemann solvers have been developed by Batten, Leschziner and Goldberg [33], who have also applied the schemes to turbulent flows. The HLLC scheme can be used as the building block for high–order methods, semi discrete, fully discrete, finite volume and discontinuous Galerkin finite element methods, on structured and unstructured grids. See for example [6], [86], [237], [334], [361], [382], [553] and [572]. At this stage, two useful remarks on the HLLC flux are worth mentioning. The first concerns the positivity/negativity of the momentum flux Safranov [420]. The second (Dr V. A. Titarev, personal communication) concerns the question of robustness of the choice of wave speeds in the HLL and HLLC solvers for the case of very high speed flow inpinging on solid stationary walls; some of the well known wave speed estimates may fail.

Perhaps the most significant advance of the HLLC approach concerns systems with more than three distinct characteristic fields, such as systems for multiphase flow and the MHD equations, for example. A proper treatment of these, following the HLLC approach, requires the construction of an appropriate wave model that includes, ideally, all the characteristic fields of the relevant system. Developments in this direction are found, for example, in [230], [474] and [75].

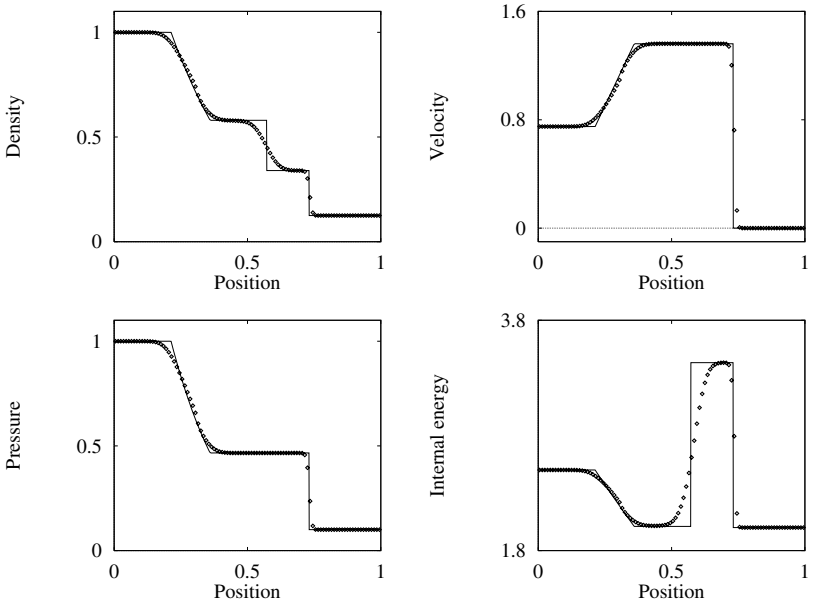

Fig. 10.5. Godunov's method with HLLC Riemann solver applied to Test 1, with $x_0 = 0.3$. Numerical (symbol) and exact (line) solutions are compared at time 0.2.

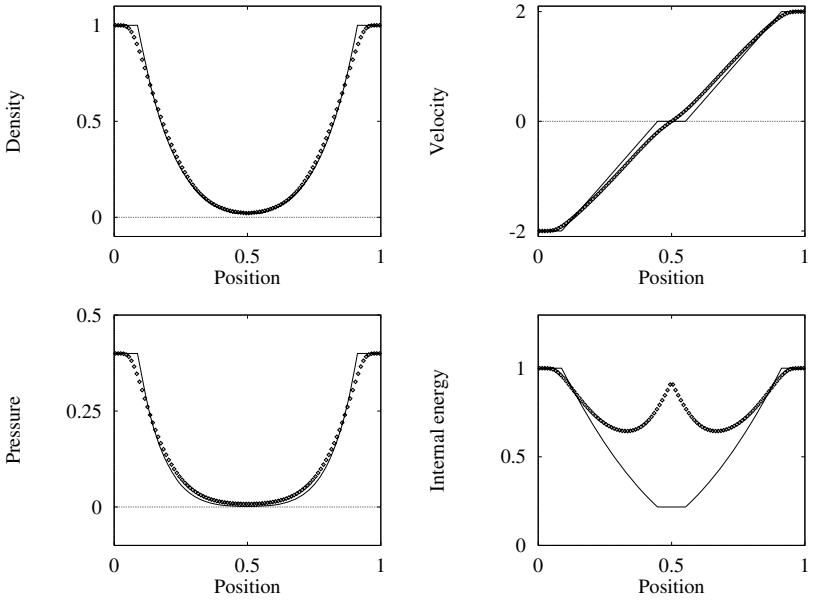

Fig. 10.6. Godunov's method with HLLC Riemann solver applied to Test 2, with $x_0 = 0.5$. Numerical (symbol) and exact (line) solutions are compared at time 0.15.

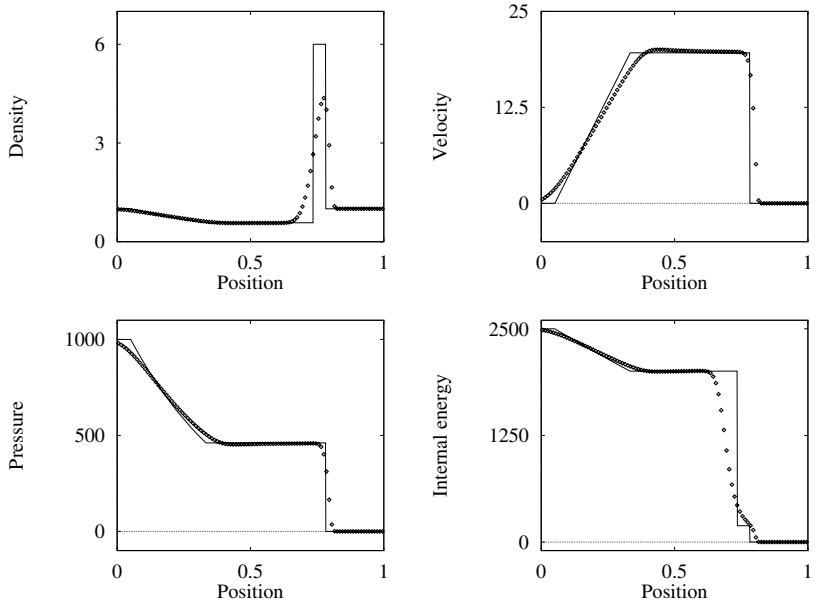

Fig. 10.7. Godunov's method with HLLC Riemann solver applied to Test 3, with $x_0 = 0.5$. Numerical (symbol) and exact (line) solutions are compared at time 0.012.

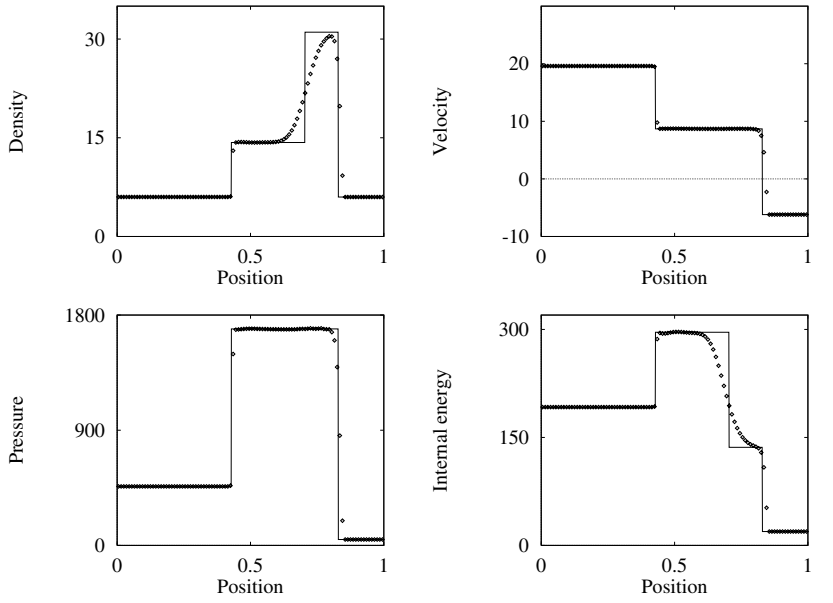

Fig. 10.8. Godunov's method with HLLC Riemann solver applied to Test 4, with $x_0 = 0.4$. Numerical (symbol) and exact (line) solutions are compared at time 0.035.

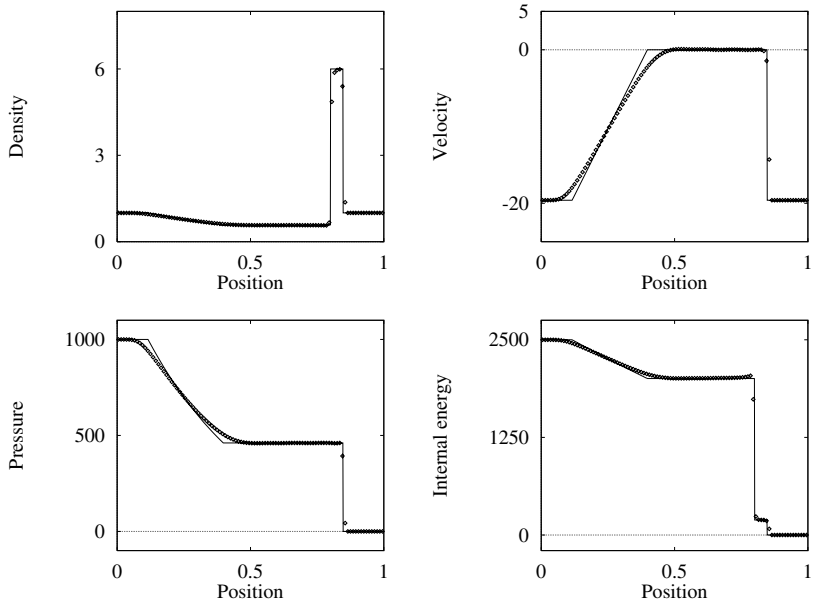

Fig. 10.9. Godunov's method with HLLC Riemann solver applied to Test 5, with $x_0 = 0.8$. Numerical (symbol) and exact (line) solutions are compared at time 0.012.

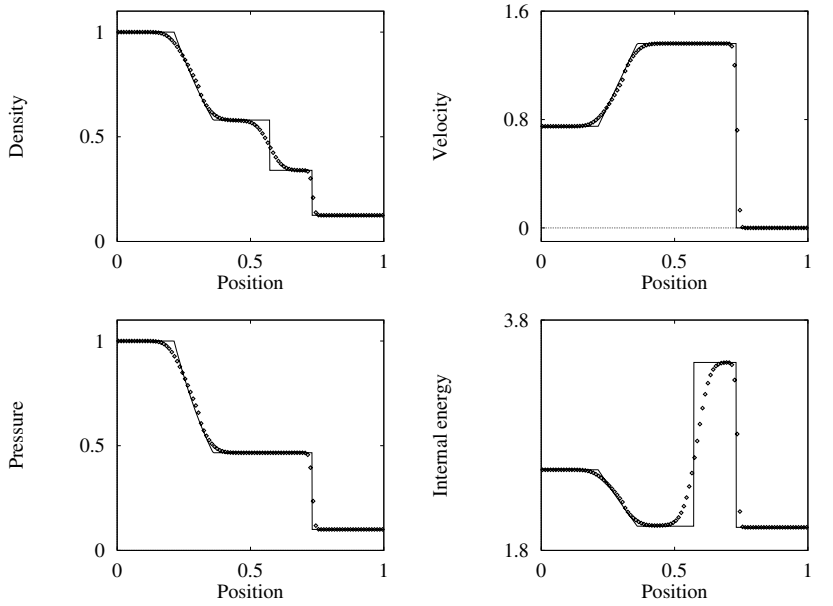

Fig. 10.10. Godunov's method with HLL Riemann solver applied to Test 1, with $x_0 = 0.3$. Numerical (symbol) and exact (line) solutions are compared at time 0.2.

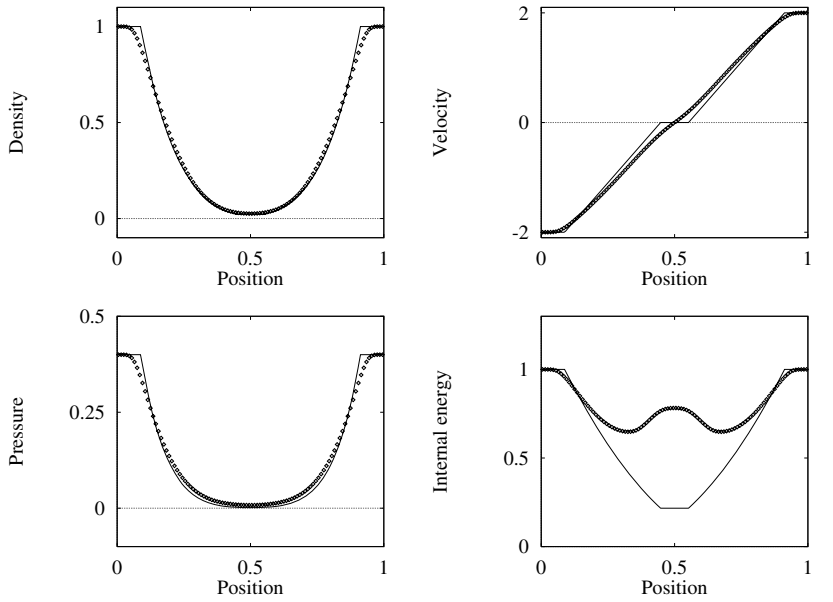

Fig. 10.11. Godunov's method with HLL Riemann solver applied to Test 2, with $x_0 = 0.5$. Numerical (symbol) and exact (line) solutions are compared at time 0.15.

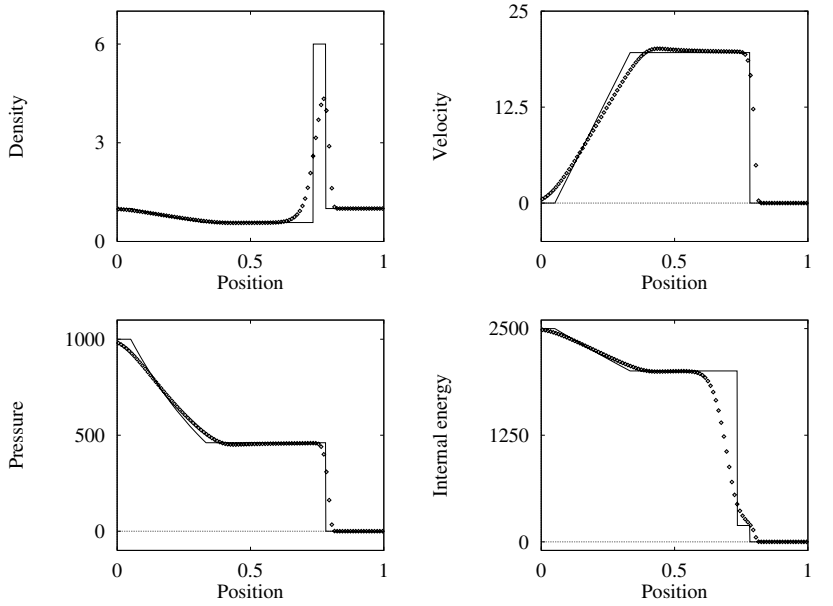

Fig. 10.12. Godunov's method with HLL Riemann solver applied to Test 3, with $x_0 = 0.5$. Numerical (symbol) and exact (line) solutions are compared at time 0.012.

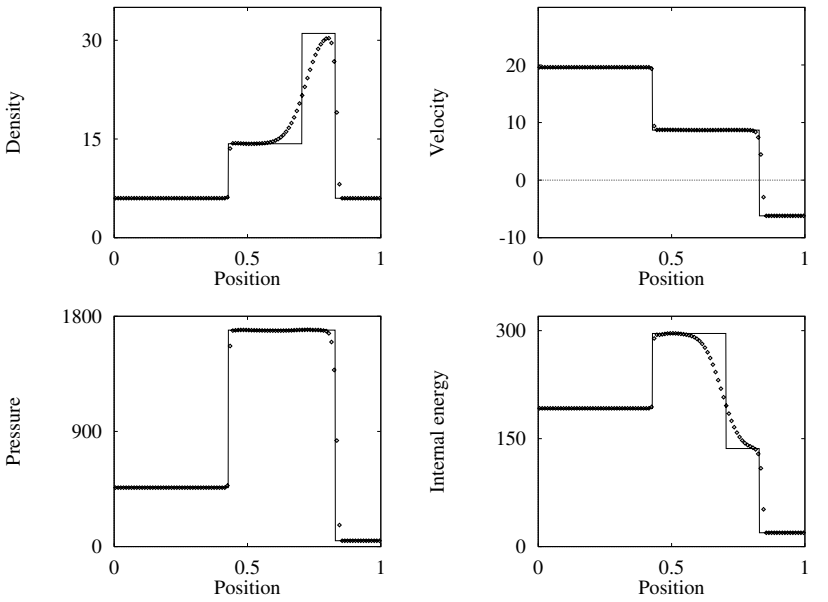

Fig. 10.13. Godunov's method with HLL Riemann solver applied to Test 4, with $x_0 = 0.4$. Numerical (symbol) and exact (line) solutions are compared at time 0.035.

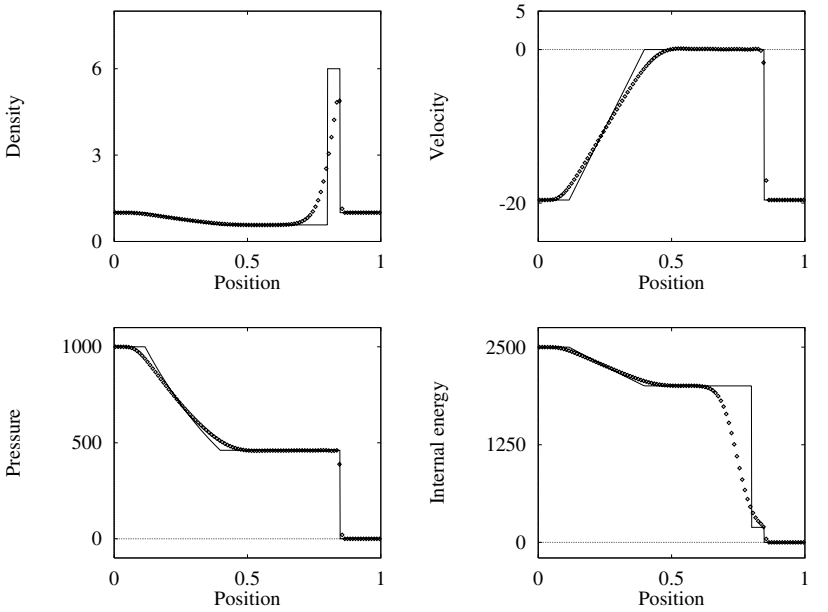

Fig. 10.14. Godunov's method with HLL Riemann solver applied to Test 5, with $x_0 = 0.8$. Numerical (symbol) and exact (line) solutions are compared at time 0.012.

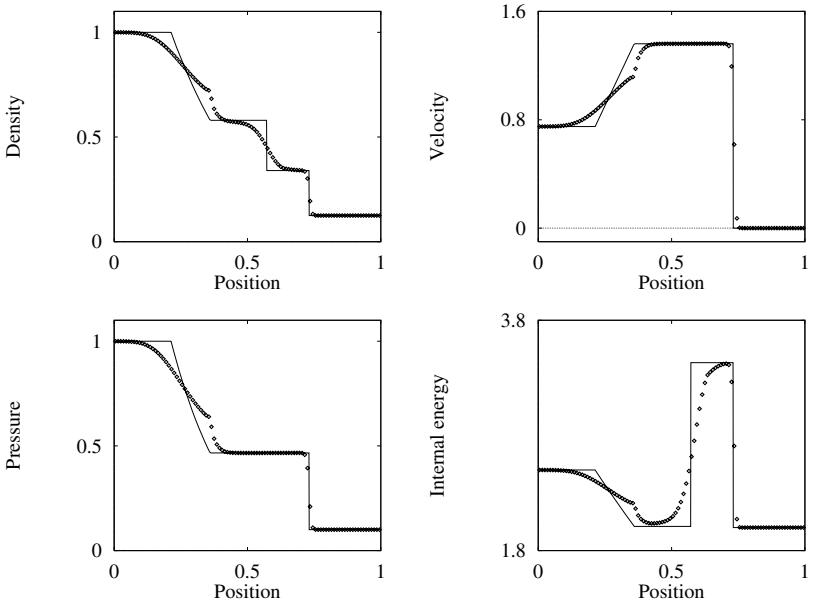

Fig. 10.15. Rusanov's method applied to Test 1, with $x_0 = 0.3$. Numerical (symbol) and exact (line) solutions are compared at time 0.2.

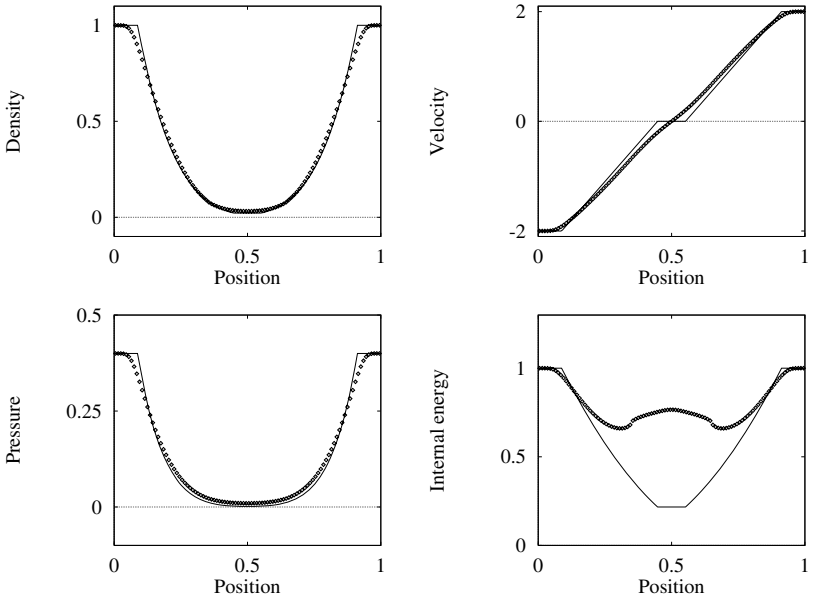

Fig. 10.16. Rusanov's method applied to Test 2, with $x_0 = 0.5$. Numerical (symbol) and exact (line) solutions are compared at time 0.15.

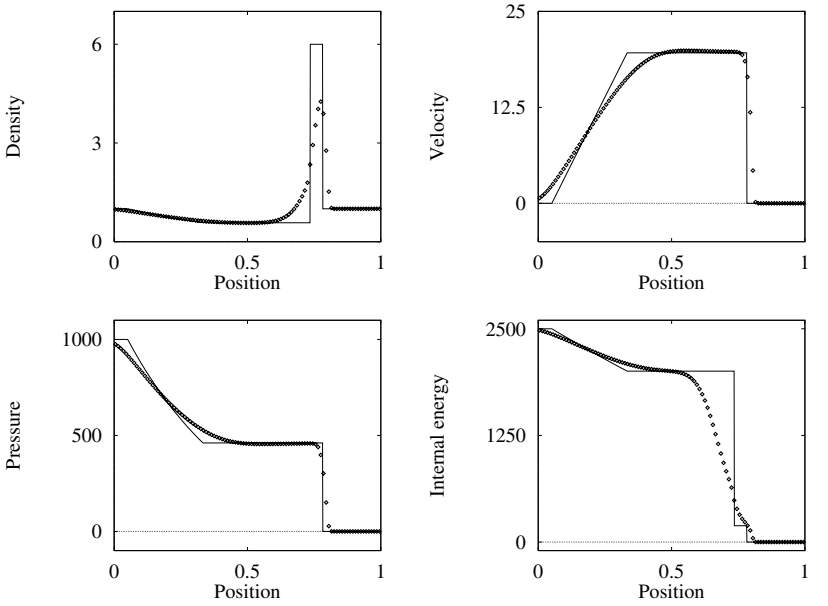

Fig. 10.17. Rusanov's method applied to Test 3, with $x_0 = 0.5$. Numerical (symbol) and exact (line) solutions are compared at time 0.012.

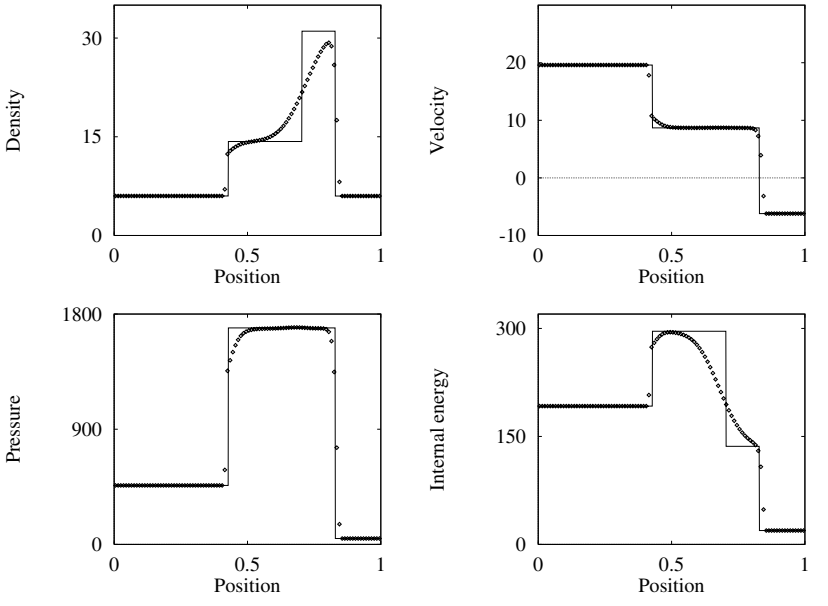

Fig. 10.18. Rusanov's method applied to Test 4, with $x_0 = 0.4$. Numerical (symbol) and exact (line) solutions are compared at time 0.035.

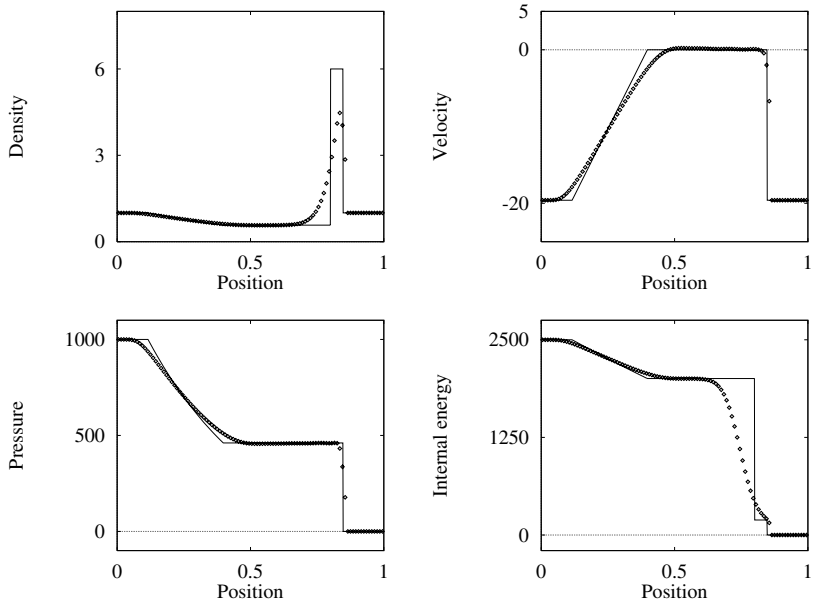

Fig. 10.19. Rusanov's method applied to Test 5, with $x_0 = 0.8$. Numerical (symbol) and exact (line) solutions are compared at time 0.012.

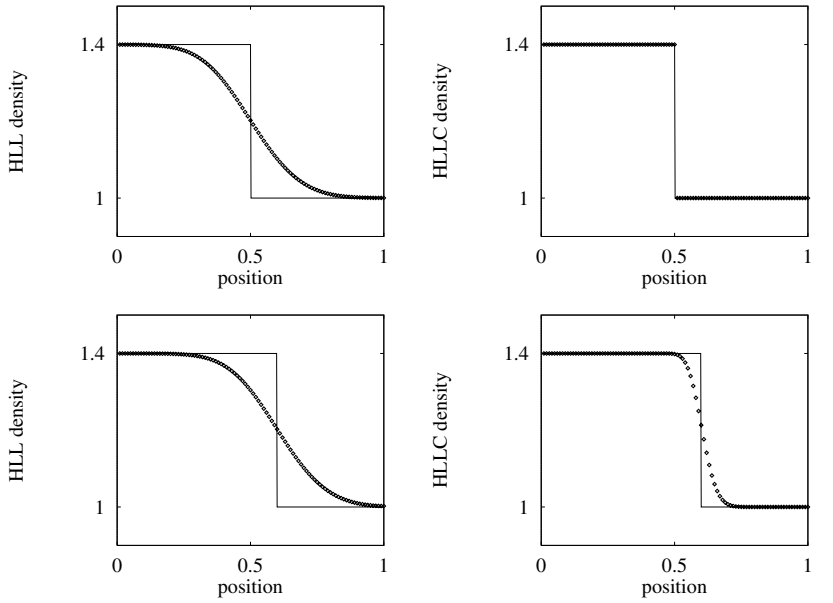

Fig. 10.20. Godunov's method with HLL (left) and HLLC (right) Riemann solvers applied to Tests 6 and 7. Numerical (symbol) and exact (line) solutions are compared at time 2.0.